The Study on Numerical Simulation of Rotor Tip Flow Field of a Transonic Compressor

Tianye Ji [a], Xie Fang, Youjun Wang and Tao Yi

Xi'an Research Institute of Hi-tech, Xi'an 710025, Shaanxi, People's Republic of China

[a]15594809968@163.com

Abstract

With the research object of NASA rotor 35, different turbulence models are applied. Four sets of grids are configured to do the single- channel numerical simulation on the rotor 35. The analysis indicates that the tip flow field of rotor 35 has no induced vortex. The main factor of impacting the track of leakage vortex is proved as the mainstream. The suitable circumferential mesh encryption and mesh encryption of the near cartridge receiver's wall are the essential condition to acquire the relatively accurate track of leakage vortex.

Keywords

Transonic Compressor; Induced Vortex; A Turbulence Model.

1. Introduction

The spiral break-up of the tip leakage vortex is the primary cause for resulting in non-stationarity in a tip area. Moreover, the disturbance will be spread along the circumferential direction, resulting in rotating stall in a compressor. The Professor Wu Yanhui[1] is based on a low-velocity axial compressor's rotors in the Northwestern Polytechnical University. The study finds that there is the Tip Secondary Vortex(TSV) in a channel under the near stall condition. The vortex is considered as being formed by the common action of tip leakage vortex's break-up, incoming flow and gap flow between adjacent fan blades. Moreover, she also finds that the formation and movement of TSV are the primary causes for resulting in non-stationarity of tip and also are inner mechanism for rotors to form sudden disturbance in stall state from the stable condition.

In the paper, with the research object of NASA rotor 35, different turbulence models are applied. Four sets of grids are configured to do the single-channel numerical simulation on the rotor 35 to verify that whether a tip area has the induced vortex.

2. Grid Calculation and Configuration of Computational Conditions

According to suggestion of Van Zante et al[2], mesh encryption of the near cartridge receiver's wall can acquire the more accurate track of the leakage flow. Zhang Zhuoxun only encrypts two grids near the cartridge receiver's wall, thus it is impossible to simulate the shearing layer of the wall accurately. On the basis of Zhang Zhuoxun's original grid, quality of the entire grid is improved, especially for closing to the end wall. Different turbulence models are applied. With the original grid, there are a total of four configurations. Parameters of four grid configurations and corresponding turbulence models are shown in Table 1.

Table 1. Parameters of Grid Configurations and Turbulence Models

	Total grids (ten thousand)	O-type grids			Tip O-type grids			Turbulence models
		I	J	k	I	J	k	
C1	64	21	73	121	17	17	121	k-epsilon
C2	180	53	77	217	25	17	217	k-epsilon
C3	240	53	97	217	25	37	217	k-epsilon
C4	240	53	97	217	25	37	217	S-A

C1 is the grid of Zhang Zhuoxun. The rest of them are new grids after improving quality. The grid distribution of four grid configurations is shown in Figure 1. C1 is divided into seven parts. C2, C3 and C4 are divided into nine parts, because front and back edges of fan blades are added with a control line. The gap grid distribution of four grid configurations is shown in Figure 2. It can be observed that C1's near wall side only has two layers of mesh encryption. The rest of grids are distributed in the gap. J-directional grid quantity in the gap of C3 and C4 is increased by one time by comparing with C1. Moreover, it is encrypted closing to the near wall side. It is distributed as the certain proportion for the distant wall side. The gap treatment of C2 is similar to C1. Others are quite the same to C3 and C4, because it aims at studying whether circumferential and flow mesh encryption will generate an obvious influence on the track of the leakage flow.

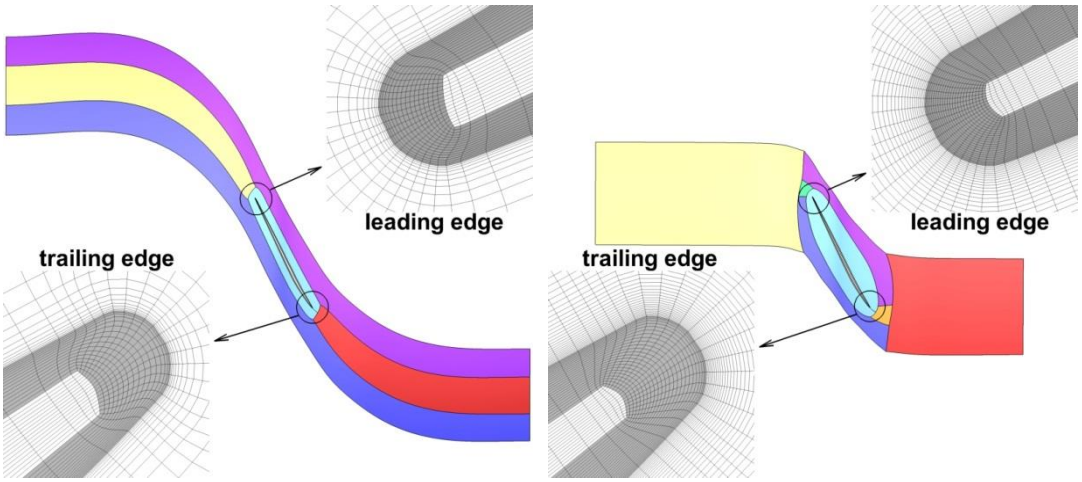

(a) C1 k-epsilon model (b) C2 k-epsilon model, C3 k-epsilon model, C4 S-A model
Fig. 1 Grid Distribution

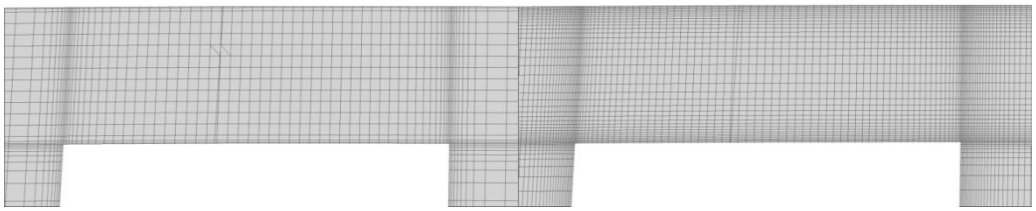

(a)C1 k-epsilon model (b) C3 k-epsilon model, C4 S-A model
Fig. 2 Gap Grid Distribution

The numerical calculation applies the Euranus solver under the commercial software named NUMECA to solve the three-dimensional Reynolds time-averaged Navier-Stokes equation under the relative coordinate system. The second-order unwind of flux difference splitting is applied. The van albada limiter is used to limit vibration of solutions. Moreover, four-order explicit Runge-kutta time matching method is applied to acquire stationary solutions. In order to improve computational efficiency, multiple accelerating convergence technologies, such as multigrid method, residual smoothing and local time step, etc., are applied. Moreover, the settings of boundary conditions are similar to Zhang Zhuoxun's settings, such as given total temperature, total pressure and flow angle(axial inlet) in line with the experimental environment for entrance, given static pressure at the mean radius for the exit, and confirmation of distributing static pressure along the radial direction as the simplified radial equilibrium equations, heat insulation and non-slipping boundary conditions for the wall, hub(axial position is between -0.2013cm and 4.1715cm) in the certain area linked with the rotor's fan blades and rotation of fan blades, other parts of the hub, and static cartridge receiver. Turbulence models apply the k-ε Yang-Shih model and Spalart-Allmaras model, respectively. For

the k-ε model, the inlet turbulent kinetic energy k and turbulent dissipation ε should be given, where k is $39m^2/s^2$, and ε is $85644m^2/s^3$.

3. Numerical Simulation Verification

The study of Van Zante et al.[3], is carried out under the condition of near peak efficiency for 80% of designed rotate velocity. Therefore, in order to conduct the effective comparison with his study, the analytical condition in the study is the condition of near peak efficiency under 80% of rotate velocity. The overall performance curve under the rotate velocity is shown in Figure 3. The overall pressure ratio curve of Figure (a) includes the computational results and experimental results. However, there is no experimental efficiency curve, so computational results are only shown in Figure (b). The peak efficiency under the curve can be obtained by calculating four grid configurations marked in Figure 3. In Figure (b), Pei(PE refers to Peak efficiency, and i corresponds to four grid configurations) is used to do more careful differentiation. It can be observed from Figure (a) that the performance curve trend of isolated rotors can be better simulated from C1 to C4. Moreover, the experimental errors are maintained in the low level. The biggest feature means that the four computational curves basically can be divided into two categories, C1, C2 and C3 based on the k-epsilon model and C4 based on S-A model. Curves from C1 to C3 are basically consistent. Curves of C3 and C3 are almost the same. Compared with the first category of curves, C4 curve based on the S-A model is obviously distinguished from them. It is closest to the experiment as the condition of mass flow. As closing to the stall boundary, it has the larger deviation from the experiment. On the contrary, it can't be better matched the first category of curves. For first category of curves, C2 only has the circumferential and flow mesh encryption by comparing with C1. By comparing with C3, C2 and C1 are only improved in the gap grid. From C1 to C2, and then to C3, grid quality and grid quantity are increased by a grade, but this has the smaller influence on the overall performance. In the Figure(b), C2 and C3 curves are almost the same. They also keep consistent with the C1 curve basically. They only have some differences as having smaller flow. Such a similarity is easy to make people misunderstand. In other words, grid improvement under the condition can't increase accuracy of flow field or may result in differences in accuracy. According to Zhang Zhuoxun's numerical verification on stage 35, the least configuration of grid quantity is greatly close to the results of previous studies. The intervention of configurations with the larger grid quantity obviously exceeds the estimation on shock wave and suction surface of the moving blades' areas, indicating that it is not enough to just observe from the performance curve. As a result, by combining with the LDV experimental data about rotor 35 studied by Van Zante et al.[4], the tip areas' flow field of four configurations under the condition of near peak efficiency will be compared and analyzed in details as follows.

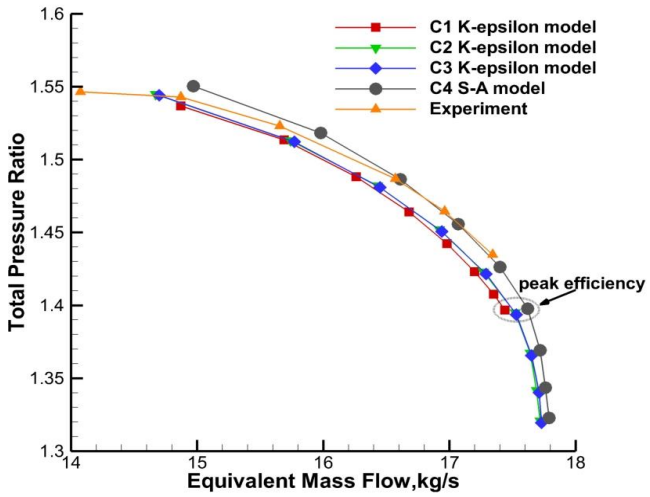

(a) Curves of Overall Pressure Ratio

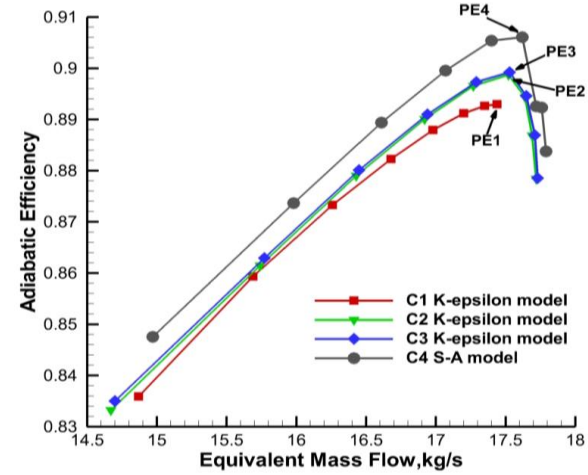

(b) Curves of Efficiency

Fig.3 Overall Performance Curves under 80% of Designed Rotate Velocity

The experiment of absolute tangential velocity and computational results at r-t section of 33% and 92% of fan blades' chord length are shown in Figure 4 and Figure 5, respectively. It should be noticed that it is only limited to the graphic processing. The section in the figure is only the r-t section at the radial chord length of the tip(vertical to z-axis). This differs from the channel section at the fan blade's chord length in the experiment. Therefore, the r-t section is close to the experimental section at the part of extremely closing to the tip. The further it gets away from the tip, the larger deviation of the section position will be. Therefore, the comparative analysis in the experiment is only restricted to the tip part. At the 33% of chord length, there is an area with the larger tangential velocity in the experimental results, namely the main leakage flow. Because the experimental data only give the velocity distribution below 97% of blade height, the bottom of the main leakage flow is only displayed. Four kinds of numerical calculations also simulate the main features of the flow field accurately. Compared with the experimental data, the computational velocity distribution is probably consistent with them, but only has a few differences in measurements. After conducting comparative analysis for four computational results, it can be observed that there is a difference in the track of main leakage flow captured by different grid configurations. Main leakage flow of C1 is the strongest and is also closest to the adjacent fan blade. The simulated results in C3 and C4 are similar. The leakage flow is the weakest and they also greatly keep away from the adjacent fan blade. Results of C2 are kept in the middle, indicating that improvement on grid quality and quantity will impact the track of leakage flow: only to do circumferential and flow mesh encryption and improvement on grid quality. For example, compared with C1, C2's track of leakage flow is moved to the suctions surface of the original fan blade. Moreover, gap grid quantity is increased and encrypted to the near cartridge receiver's wall grid. For example, compared with C1 and C2, C3 and C4's track of leakage flow is obviously closer to the suction surface of the original fan blade. Such findings are consistent with Van Zante's conclusions, so that the author hopes these changes also will be caused by the induced vortex.

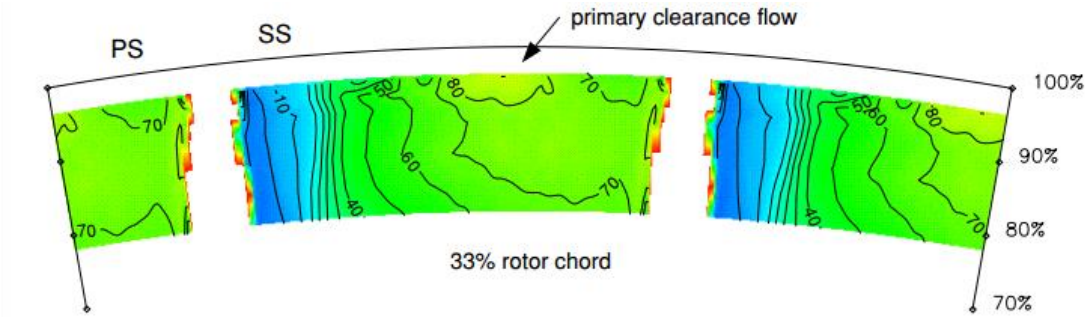

(a) Experimental Results

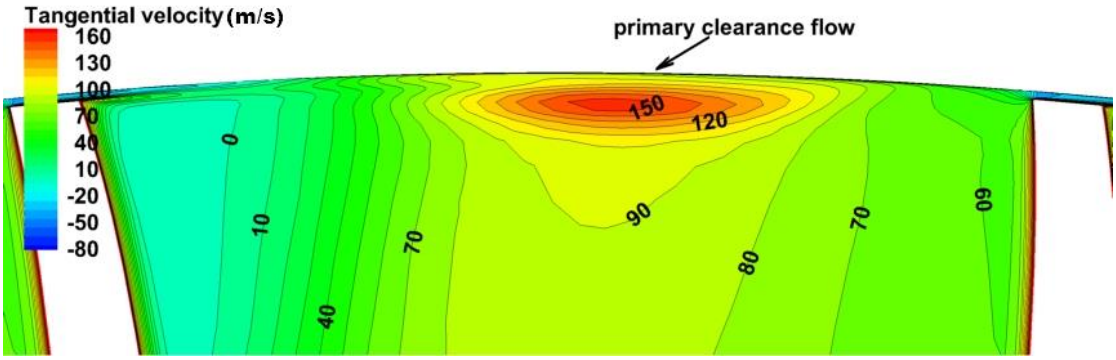

(b)C1 k-epsilon model

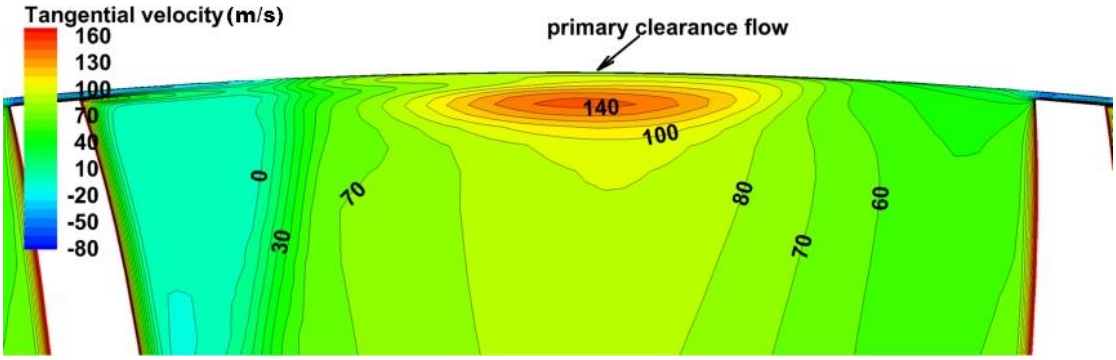

(c)C2 k-epsilon model

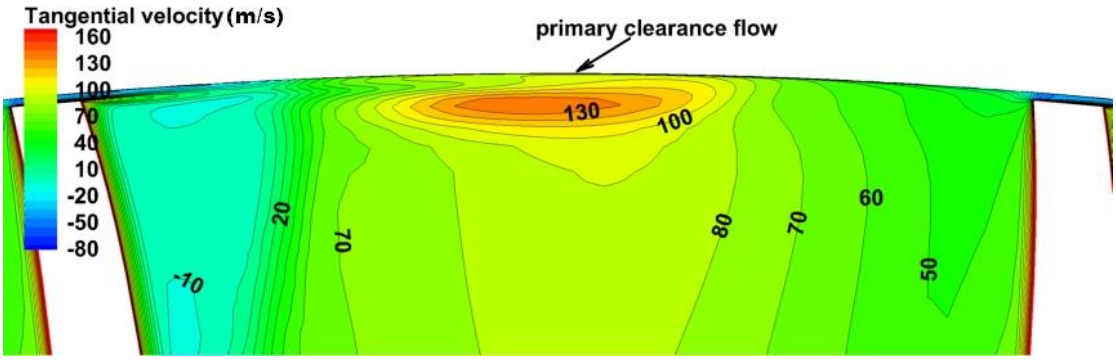

(d)C3 k-epsilon model

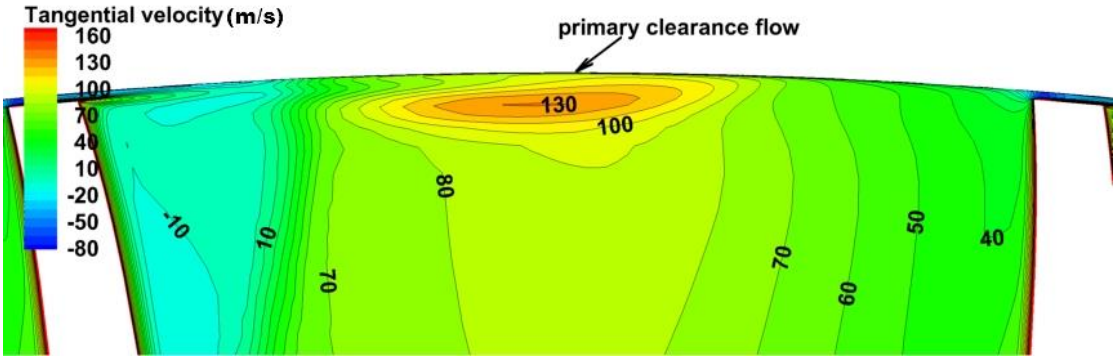

(e)C4 S-A model

Fig. 4 The Absolute Tangential Velocity (m/s) Distribution at the r-t Section of 33% of Blade's Chord Length

At the 92% of chord length, there is another characteristic phenomenon near the suction surface of the tip: secondary leakage flow. The secondary leakage flow is firstly discovered by Suder and Celestina[5] under the rotate velocity of the rotor 37. Gerolymos[6] and Vallet[7] also found the same phenomenon under the design rotate velocity of the motor 37. They thought that the secondary leakage was formed by tip leakage flow clipping boundary layer of the suction surface to move to the

tip radial direction. However, in all numerical simulation of Van Zante[8], there is no radial direction migration on the boundary layer of the suction surface. Thus, he thought that the occurrence of such a phenomenon was only caused by the leakage flow at the rear fan blade. In the study, it abides by the opinions of Van Zante. It can be observed from Figure5(a) that though the main leakage flow is close to the pressure surface of the adjacent fan blade, it isn't stacked on the side of the pressure surface. Influences of different grid configurations on the track of the main leakage flow are shown in Figures(b), (c) and (d). C3 is the closest to the experiment. C1 has the biggest experimental errors, indicating that the track of the main leakage flow is too close to the pressure surface of the adjacent fan blade. In addition, it also can be observed that by comparing with the experimental results, the results of numerical simulation underestimate the strength of main leakage flow. It seems that different models have the smaller influences on the track of main leakage flow. The channel positions of C3 and C4's leakage flow at 33% and 92% of chord length are almost consistent. The only difference means that the estimated gap flow strength of S-A model is smaller than the K-epsilon model.

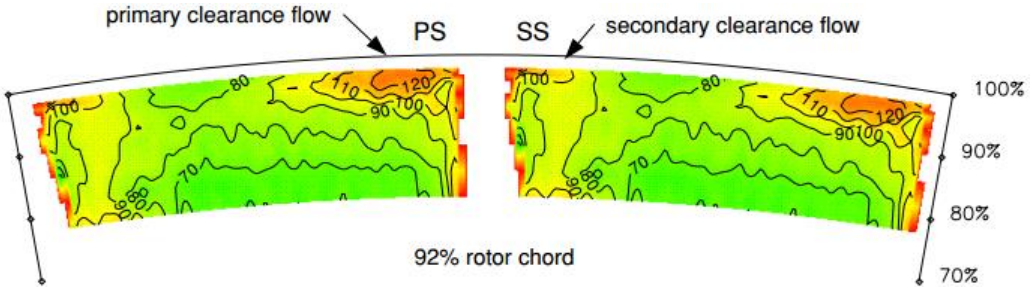

(a) Experimental Results

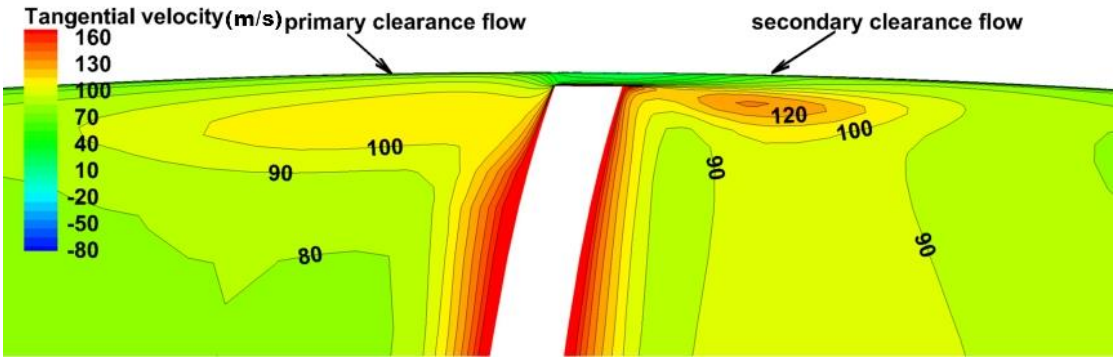

(b)C1 k-epsilon model

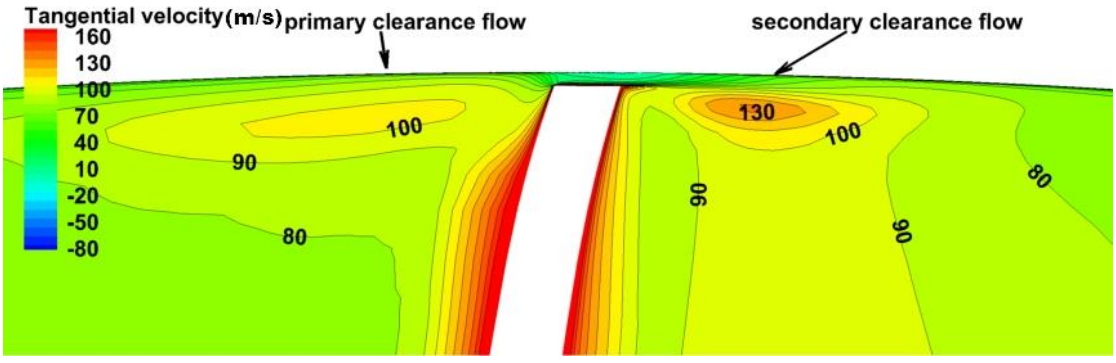

(c)C2 k-epsilon model

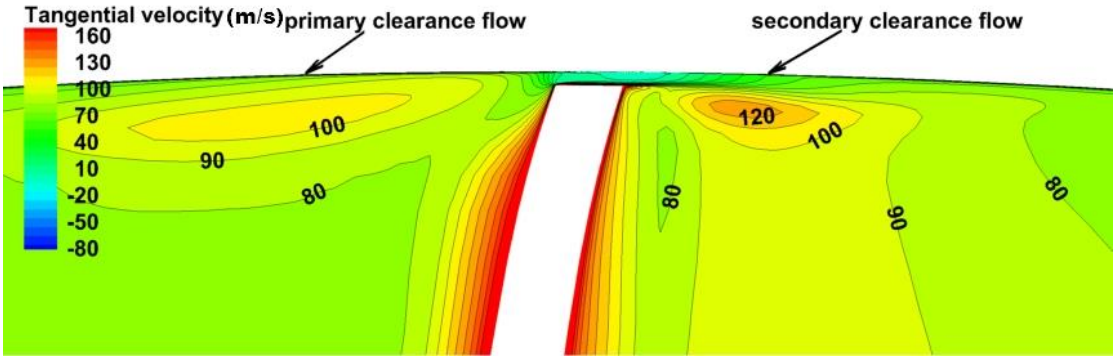

(d)C3 k-epsilon model

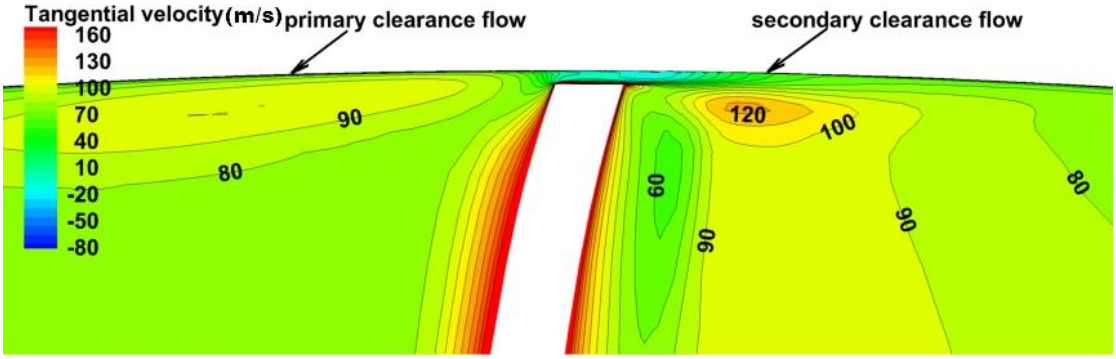

(e)C4 S-A model

Fig. 5 The Absolute Tangential Velocity (m/s) Distribution at the r-t Section of 92% of Blade's Chord Length

4. Conclusion

By combining with existing experimental data, the computational results of four grid configurations are compared and analyzed. Conclusions are drawn as follows:

1. Suitable circumferential grid distribution and mesh encryption of near cartridge receiver's wall are the key to simulate the track of the leakage vortex accurately. Different turbulence models bring about the smaller difference on it.

2. Under 80% of designed rotate velocity, there is not induced vortex in the tip flow field of the motor 35. There are universal induced tracks. The probable formative process can be described as: after incoming flow breaks away from the shearing layer of the cartridge receiver's wall under the rolling of the leakage vortex, velocity is reduced and it pulls back and steers by the leakage vortex, resulting in forming the upper narrow low-speed area out of the leakage vortex and reducing the flux section of the cartridge receiver, so as to speed up the incoming flow in this part, form the area with the larger paraxial velocity in parallel development. The track of the leakage vortex is also the result after being balanced with the area.

References

[1]Wu Y, Chu W. Behaviour of tip-leakage flow in an axial flow compressor rotor[J]. Proceedings of the Institution of Mechanical Engineers, Part A: Journal of Power and Energy, 2007, 221(1): 99-110.

[2] Van Zante, D. E., Strazisar, A. J., Wood, J. R., Hathaway, M. D., Okiishi, T. H., 2000, Recommendations for Achieving Numerical Simulation of Tip Clearance flows in Transonic Compressor Rotors, ASME Journal of Turbomachinery, 122, pp. 733-742.

[3] Wu Y, Li Q, Chu W, et al. Numerical investigation of the unsteady behaviour of tip clearance flow and its possible link to stall inception[J]. Proceedings of the Institution of Mechanical Engineers, Part A: Journal of Power and Energy, 2010, 224(1): 85-96.

[4] XIE Fang, CHU Wu-li, ZHANG Hao-guan, Influence shock waves leakage vortex boundary layer separation interaction in a single- stage transonic axial compressor[J] , 2012.27(2),425-430.
[5] Suder, K. L. and Celestina, M. L., 1996, Experimental and Computational Investigation of the Tip Clearance Flow in a Transonic Axial Compressor Rotor, ASME Journal of Turbomachinery, Vol. 118, pp. 218-229.
[6] Gerolymos, G.A. and Vallet, I., 1998, Tip-Clearance and Secondary Flows in a Transonic Compressor Rotor, ASME Paper 98-GT-366.
[7] Reid L , Moore R D. Performance of as ingle-stage axial-flow tran sonic co mpressor with rotor and stator aspect ratios o f 1. 19 and 1. 26, respectively , and with design pressure ratio of 1. 82 . N A SA TP - 1338, 1978.
[8] Gupta A, Khalid S A, McNulty G S, et al. Prediction of Low Speed Compressor Rotor Flowfields With Large Tip Clearances[C]//ASME Turbo Expo 2003, collocated with the 2003 International Joint Power Generation Conference. American Society of Mechanical Engineers, 2003: 1135-1145.